Magnetic Field in a Transverse- and Axial-flux Permanent-Magnet Synchronous Generator from 3-D FEA

T. F. Chan[1], Weimin Wang[1] and L. L. Lai[2]
[1]Department of EE, the Hong Kong Polytechnic University, Hung Hom, Hong Kong, China
[2]Energy Systems Group, School of Mathematics and Engineering Sciences, City University London, UK
eetfchan@polyu.edu.hk,

Abstract — The magnet field in a transverse- and axial-flux permanent-magnet generator is studied. In this novel machine, the main flux flows in the transverse direction as the rotation. The flux density distribution is analyzed using a three-dimensional finite element method (3-D FEM). Experimental flux density measurements are in good agreement with the computed results. Using a time-stepping technique, the output voltage is also computed.

I. Introduction

The axial-flux permanent-magnet synchronous generator (AFPMSG) is considered a suitable energy converter for direct-coupled wind turbine applications [1],[2]. Most AFPMSG designs employ the longitudinal flux design, i.e. the main flux flows in plane parallel to the rotational direction [2],[3],[4]. In this paper, a transverse-flux AFPMSG design is proposed and investigated. Fig. 1 shows the assembled view of the prototype generator. 16 pole pieces are mounted circumferentially on a non-magnetic disk. Each pole piece is C-shaped and carries a permanent magnet on the bottom yoke, while the top yoke is detachable to facilitate assembly. The stator disk winding is iron-coreless consists of 12 single-layer coils embedded in epoxy resin. The winding is supported by a stationary shaft and is sandwiched between the top rotor yokes and the permanent magnets. As shown in Fig. 2, the flux is mainly confined to each pole piece and flows in the transverse direction as the rotor movement. The flux density distribution is inherently three-dimensional. In this paper, a time-stepping, coupled field-circuit, three-dimensional finite element method is used for analyzing this prototype transverse-flux AFPMSG.

II. Analysis

The three-dimensional (3-D) finite element transient solver of ANSYS Version 11 SP1 was used as the analysis tool. For computation of the no-load magnetic field quantities a static field solution is sufficient. For computation of the generator performance on load, a time-stepping analysis is needed.

Since the pole number to stator coil ratio is 16/12, the resultant field pattern will repeat over every four pole-pitches when the AFPMSG is on load. Thus the minimum number of poles to be modeled should be four for periodic boundary conditions to be applied. Fig. 3 shows the geometric model of the transverse-flux AFPMSG, showing the sliding surface for time-stepping FEA. The meshed areas in black are the pole pieces and the meshed areas in gray represent the air space. The rotor magnets are embedded in the rotor surface and the armature coils are embedded in the stator surface in Fig. 3.

The stator and rotor interfaces are meshed with 20 elements in the radial direction, 45 elements in the circumferential direction, and 3 elements in the axial direction. The step size of rotor movement is thus equivalent to 2 mechanical degrees. With the mesh chosen, the total number of finite elements is 28705. On a Sun Microsystems E6900 (CPU 4 x 900 MHz + 64 bits Processor Memory 4GB), it took approximately 120 hours for a time-stepping analysis for a given load.

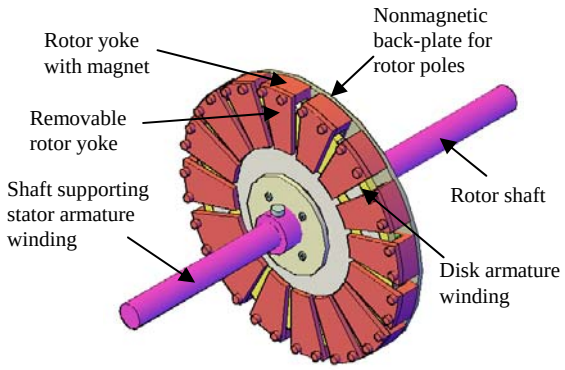

Fig. 1. Assembled view of the experimental AFPMSG

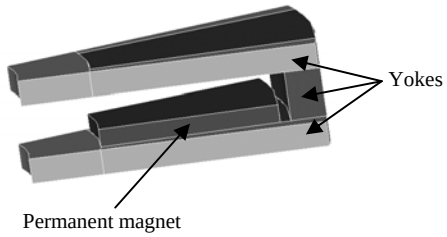

Fig. 2. Geometric model of one pole of the AFPMSG

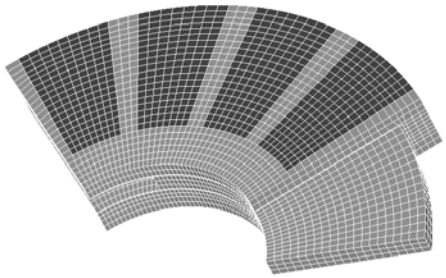

Fig. 3. Definition of the sliding surface for time-stepping 3-D FEA

III. RESULTS

A. Surface plots of air gap flux density

In the subsequent discussion r, θ and z denote, respectively, the radial, circumferential and axial directions of the AFPMSG. Fig. 4 shows the computed surface plots of the air gap flux density components in the AFPMSG under no load conditions, where circumferential distances 0^0 and 180^0 coincide with the interpolar axes. Fig. 4a shows that the axial flux density component B_z decreases significantly at the inner and outer radii of the AFPMSG. The value of B_r is small under a magnetic pole, but due to fringing flux in the radial directions at the outer radii there is a sharp peak at r = 0.013 m (Fig. 4b).

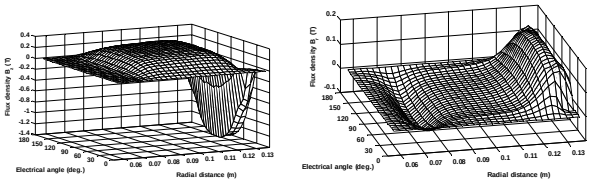

(a) (b)

Fig. 4. Surface plots of no-load flux density components at mid-plane of armature winding: (a) axial; (b) radial

B. Effect of axial position on flux density

Fig. 5 shows the circumferential and radial variations of B_z. The variation of B_z in the circumferential direction affects principally the magnitude and waveform of the generated emf. At z = 13 mm (1 mm above the surface of magnet), the B_z waveform is approximately trapezoidal but as z increases the waveform gradually becomes more rounded, At z = 21 mm (1 mm below the top rotor yoke), B_z decreases in magnitude but the waveform becomes closer to a sinusoid. (Fig. 5a). As shown in Fig. 5b, B_z is almost constant along the center line of the magnet at z = 13 mm, but as z increases fringing effect at the inner and outer edges of the magnet becomes prominent, resulting in considerable decrease in flux density. The flux returns largely in the connecting yoke between the upper and rotor back plates, hence the reversal in sign of B_z. As shown in Fig. 6, experimental field measurement results are in good agreement with computed results.

C. Computed voltage waveforms

Fig. 7 shows the computed waveforms of the phase and line voltages when the AFPMSG is supplying a resistive load of 20 Ω per phase at rated speed. It is found that the phase voltages are flat-topped, due mainly to third harmonic contents in the air gap flux density B_z as well as effect of armature reaction. The line voltages, however, are sinusoidal since a three-phase three-wire star-connected load is being supplied. Convergence of the 3D FEA computations is fast: in a few steps the computed values are already very close to those at steady state.

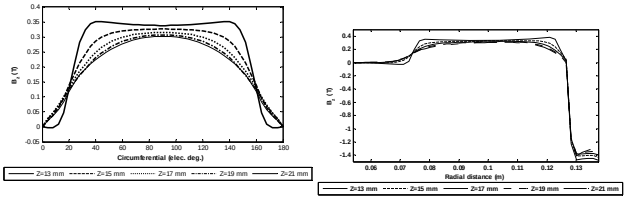

(a) (b)

Fig. 5. Variation of B_z with axial position in the air gap region: (a) along circumferential direction at mean radius; (b) along radial direction at pole center

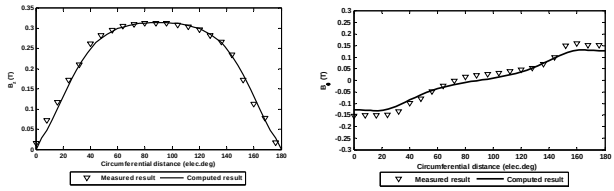

Fig. 6 Variation of B_z and B_θ at z = 17 mm of AFPMSG on no load (a) B_z; (b) B_θ

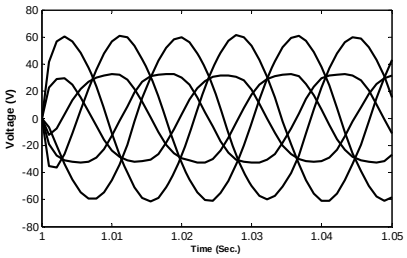

Fig. 7. Computed waveforms of phase and line voltages when the AFPMSG is supplying a load of 20 Ω per phase at 300 r/min

IV. CONCLUSIONS

Further details of field analysis and experimental results on the transverse- and axial-flux permanent-magnet synchronous generator will be reported in the extended paper.

V. ACKNOWLEDGMENT

The work described in this paper was fully supported by a grant from the Research Committee, The Hong Kong Polytechnic University, Hong Kong, China (Project No. G-U742).

VI. REFERENCES

[1] J. R. Bumby, R. Martin, M. A. Mueller, E. Spooner, N. L. Brown and B. J. Chalmers, "Electromagnetic design of axial-flux permanent magnet machines," *IEE Proc. – Elect. Power Appl.*, 151(2), pp. 151–159, 2004.

[2] T. F. Chan and L. L. Lai, "An axial-flux permanent-magnet synchronous generator for a direct-coupled wind turbine system," *IEEE Trans. Energy Convers.*, vol. 22, no. 1, pp. 86–94, 2007.

[3] J. Azzouzi, G. Barakat and B. Dakyo, "Quasi-3-D analytical modelling of the magnetic field of an axial-flux permanent-magnet synchronous machine," *IEEE Trans. Energy Convers.*, vol. 20, no. 4, Dec. 2005, pp. 748–752

[4] Sang-Ho Lee, Su-Beom Park, Soon-O Kwon, Ji-Young Lee, Jung-Jong Lee, Jung-Pyo Hong and Jin Hur, "Characteristic analysis of the slotless axial-flux type brushless DC motors using image method," *IEEE Trans. Magn.*, vol. 42, no. 4, Apr. 2006, 1327-1330.